Acta Crystallographica Section D
Biological Crystallography
ISSN 1399-0047

Structures of K42N and K42Y sperm whale myoglobins point to an inhibitory role of distal water in peroxidase activity

Chunxue Wang,[a] Leslie L. Lovelace,[a] Shengfang Sun,[a] John H. Dawson[a,b]* and Lukasz Lebioda[a,c]*

[a]Department of Chemistry and Biochemistry, University of South Carolina, Columbia, SC 29208, USA, [b]School of Medicine, University of South Carolina, Columbia, SC 20208, USA, and [c]South Carolina Colon Cancer Center, University of South Carolina, Columbia, SC 20208, USA

Correspondence e-mail: jdawson@mailbox.sc.edu, lebioda@mailbox.sc.edu

Received 27 March 2014
Accepted 1 August 2014

PDB references: sperm whale myoglobin, K42N mutant, 4of9; K42Y mutant, 4ood

Sperm whale myoglobin (Mb) functions as an oxygen-storage protein, but in the ferric state it possesses a weak peroxidase activity which enables it to carry out H_2O_2-dependent dehalogenation reactions. Hemoglobin/dehaloperoxidase from *Amphitrite ornata* (DHP) is a dual-function protein represented by two isoproteins DHP A and DHP B; its peroxidase activity is at least ten times stronger than that of Mb and plays a physiological role. The 'DHP A-like' K42Y Mb mutant (K42Y) and the 'DHP B-like' K42N mutant (K42N) were engineered in sperm whale Mb to mimic the extended heme environments of DHP A and DHP B, respectively. The peroxidase reaction rates increased ∼3.5-fold and ∼5.5-fold in K42Y and K42N *versus* Mb, respectively. The crystal structures of the K42Y and K42N mutants revealed that the substitutions at position 42 slightly elongate not only the distances between the distal His55 and the heme iron but also the hydrogen-bonding distances between His55 and the Fe-coordinated water. The enhanced peroxidase activity of K42Y and K42N thus might be attributed in part to the weaker binding of the axial water molecule that competes with hydrogen peroxide for the binding site at the heme in the ferric state. This is likely to be the mechanism by which the relationship 'longer distal histidine to Fe distance – better peroxidase activity', which was previously proposed for heme proteins by Matsui *et al.* (1999) (*J. Biol. Chem.* **274**, 2838–2844), works. Furthermore, positive cooperativity in K42N was observed when its dehaloperoxidase activity was measured as a function of the concentration of the substrate trichlorophenol. This serendipitously engineered cooperativity was rationalized by K42N dimerization through the formation of a dityrosine bond induced by excess H_2O_2.

1. Introduction

Sperm whale myoglobin (Mb), a monomeric heme protein of 153 amino acids, has been intensively and thoughtfully studied during the past several decades. It functions as an oxygen-storage protein by reversibly binding dioxygen in the ferrous state (Antonini & Brunori, 1971). More recently, Mb was found to carry out the oxidative dehalogenation of halophenols in the presence of hydrogen peroxide when its heme is in the ferric state, although no physiological significance has been linked to this property (Osborne *et al.*, 2007; Du *et al.*, 2011). Hemoglobin/dehaloperoxidase (DHP) discovered in *Amphitrite ornata* is a homodimeric globin which consists of 137 amino acids in each subunit (Chen *et al.*, 1996; Lebioda *et al.*, 1999; LaCount *et al.*, 2000). Although the positions of the

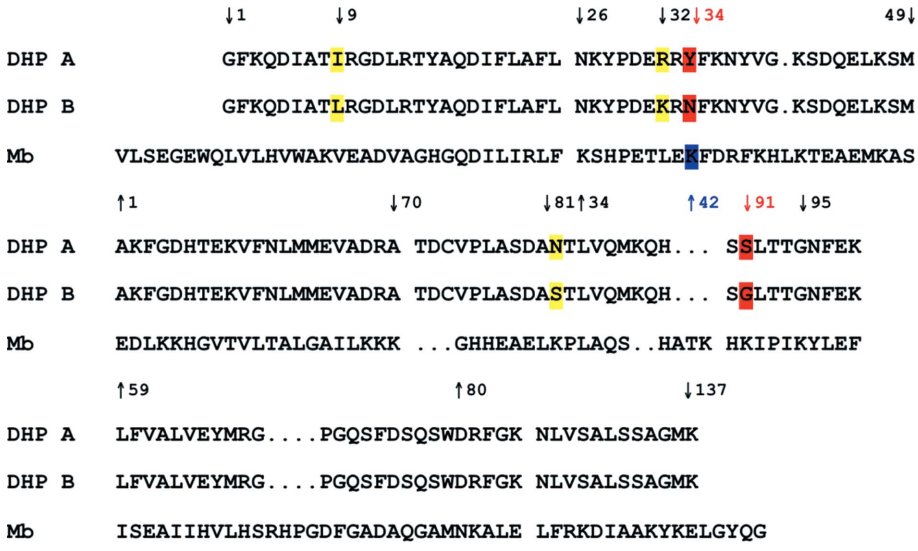

Figure 1
Amino-acid sequence alignment of DHP A, DHP B and Mb. The amino-acid differences at positions 34 and 91 between DHP A and DHP B are highlighted in red and a further three differences at positions 9, 32 and 81 are highlighted in yellow. Lys42 in Mb, which corresponds to the amino acid at position 34 in DHP, is shown in blue.

proximal histidine are significantly different (its imidazole chain is rotated by 60°; Lebioda, 2000), DHP has nearly identical spectral properties to those of Mb (Zhang *et al.* 1996; Roach *et al.*, 1997; Franzen *et al.*, 1998), reflecting the close similarities between the heme iron properties.

DHP has two physiological functions: its primary function is as an oxygen carrier to store and transport oxygen and its secondary function is as a dehaloperoxidase enzyme (Du *et al.*, 2010; Franzen *et al.*, 2012). The peroxidase activity of DHP is over one order of magnitude higher than that of Mb and its oxygen affinity is about tenfold lower than that of Mb (Osborne *et al.*, 2006, 2007; Du *et al.*, 2011; Sun *et al.*, 2014). Watanabe and coworkers noticed that the distance between the N^{ε} atom of the distal histidine and the heme Fe is longer in peroxidases than in globins (Matsui *et al.*, 1999). They engineered a double Mb mutant F43H/H64L which indeed had the distal histidine further from the heme and an increased peroxidase activity. A similar relationship was observed in a series of DHP mutants (Du *et al.*, 2010). However, the Mb F43H/H64L mutant represents a drastic rearrangement of the distal cavity. The objective of this study was to use DHP as a paradigm to increase the peroxidase activity of Mb and follow the structural factors that affect its catalytic properties. A similar approach was used to enhance dioxygen binding by making sperm whale myoglobin similar to the high-affinity *Askaris* hemoglobin (Draghi *et al.*, 2002).

The dehaloperoxidative activity of DHP B with 2,4,6-trichlorophenol as the substrate is approximately twice that of DHP A. The Y34N substitution in DHP A, *i.e.* making it somewhat DHP B-like, increases the k_{cat} values for the reaction from 63 ± 4 min^{-1} in DHP A to 85 ± 12 min^{-1} in Y34N DHP A at pH 7 and 4°C (Wang *et al.*, 2013). The amino-acid alignment of DHP A and DHP B with Mb shown in Fig. 1 indicates that Lys42 in Mb corresponds to Tyr34 in DHP A and Asn34 in DHP B, respectively. In order to test whether this residue is also important for the peroxidative function of Mb, Mb variants K42Y and K42N that mimic DHP A and DHP B, respectively, at position 34 were generated and studied. In general, intracellular peroxidase activity which generates active oxygen species is considered to be harmful. The crystal structures of the K42Y and K42N mutants of sperm whale Mb reported here (K42Y and K42N), their peroxidase activities and oxygen-binding affinities suggest that one of the mechanisms to maintain low peroxidase activity is the strong binding of distal water by ferric Mb.

2. Materials and methods

2.1. Site-directed mutagenesis and protein purification

The Mb mutants were generated using the QuikChange method. The sequences of the mutagenic primers are listed in Supplementary Table S1[1]. The pUC19 plasmid containing wild-type sperm whale Mb was a gift from Yoshi Watanabe (Institute of Molecular Science, Nagoya University, Japan). DNA with the desired mutations was verified by LI-COR DNA sequencing (Engencore at the University of South Carolina) and was then transformed into *Escherichia coli* BL21 (DE3) cells. Mb mutants were overexpressed in *E. coli* BL21 (DE3) cells and purified using an established protocol (Springer & Sligar, 1987; Huang *et al.*, 2012).

Homogenous Mb proteins in the ferric state were prepared by adding potassium ferricyanide as described previously (Qin *et al.*, 2006). Excess ferricyanide was removed using a Bio-Gel P-6 DG desalting column with 100 m*M* potassium phosphate buffer pH 7 at 4°C.

[1] Supporting information has been deposited in the IUCr electronic archive (Reference: LV5068).

Table 1
Crystallographic data and refinement statistics for Mb mutants.

Values in parentheses are for the highest resolution shell.

DHP mutant	K42Y	K42N
PDB code	4ood	4of9
X-ray source	SER-CAT 22-ID, APS	SER-CAT 22-ID, APS
Wavelength (Å)	1.0000	1.0000
No. of frames	125	110
Oscillation range (°)	1.0	1.0
Temperature (K)	100	100
Space group	$P2_12_12_1$	$P6$
Unit-cell parameters		
a (Å)	35.002	90.304
b (Å)	47.515	90.304
c (Å)	85.243	45.314
Volume (Å^3)	141770	320020
Matthews coefficient (Å^3 Da^{-1})	2.05	3.11
Solvent content (%)	40.0	60.4
Mosaicity (°)	0.3	0.3
Resolution range (Å)	42.6–1.24 (1.26–1.24)	78.2–1.24 (1.26–1.24)
Multiplicity	4.0 (1.9)	5.8 (2.1)
$\langle I/\sigma(I)\rangle$	40.7 (2.8)	36.1 (3.8)
Total No. of reflections	154441	343048
No. of unique reflections	38881	58965
Completeness (%)	93.6 (54.1)	98.8 (90.4)
$R_{\rm merge}$† (%)	4.8 (25.7)	5.8 (20.9)
R (%)	14.0 (21.0)	10.8 (15.7)
$R_{\rm free}$ (%)	19.5 (27.5)	13.1 (16.8)
R.m.s. deviation, bond lengths (Å)	0.022	0.026
R.m.s. deviation, bond angles (°)	2.4	2.5
Estimated overall coordinate error		
Based on R (Å)	0.047	0.027
Based on maximum likelihood (Å)	0.034	0.014
Ramachandran statistics, residues in (%)		
Most favored regions	98	98
Additional allowed regions	2	2
Generously allowed regions	0	0
Disallowed regions	0	0
Average B for protein (Å^2)	16.7	12.6
Average B for solvent (Å^2)	33.7	33.9

† $R_{\rm merge} = 100 \times \sum_{hkl}\sum_i |I_i(hkl) - \langle I(hkl)\rangle| / \sum_{hkl}\sum_i I_i(hkl)$, where $I_i(hkl)$ is the observed intensity and $\langle I(hkl)\rangle$ is the mean intensity of reflection hkl over all measurements of $I_i(hkl)$.

2.2. Crystallization

The proteins were buffer-exchanged into 20 m*M* Tris pH 9.0 and concentrated to 20 mg ml^{-1}. For crystallization, 2 µl protein solution was mixed with 2 µl 20 m*M* Tris pH 8.5 or 9.0, 1 m*M* EDTA and 2.6–2.8 *M* ammonium sulfate solution as reported previously (Springer *et al.*, 1989; Du *et al.*, 2011). The best crystals of K42Y and K42N were grown using the hanging-drop method at 277 K. The crystals were transferred into a cryoprotectant consisting of the mother liquor with an additional 20% ethylene glycol and were subsequently flash-cooled in liquid nitrogen.

2.3. Data collection and structure determination

All X-ray diffraction data were collected at a wavelength of 1.0000 Å on the SER-CAT 22-ID beamline at the Advanced Photon Source (APS) at Argonne National Laboratory and were then processed using the *HKL*-2000 suite (Otwinowski & Minor, 1997). The structures were determined by molecular replacement with *Phaser* from the *CCP*4 software suite (Winn *et al.*, 2011). The Mb G65T structure (PDB entry 3ock; Huang *et al.*, 2012) was utilized as the starting model for solving the structures of the other Mb mutants. Model rebuilding was carried out using *Coot* (Emsley *et al.*, 2010) and *TURBO-FRODO* (Roussel & Cambillau, 1989). Refinements were performed using *REFMAC*5 v.5.8.0069 (Murshudov *et al.*, 2011) from the *CCP*4 suite with standard restraints. The parameters and statistics of data collection and processing are summarized in Table 1. Superpositions were conducted using *LSQKAB* (Kabsch, 1976) from the *CCP*4 suite. Figs. 2 and 3 and Supplementary Figs. S2–S4 were prepared using *TURBO-FRODO*. Supplementary Figs. S1 and S8 were prepared using *PyMOL*.

2.4. Dehaloperoxidase activity assay

The dehaloperoxidase activity assay was performed on a Cary 400 spectrophotometer at 4°C using a UV–Vis absorption spectroscopic assay as described previously (Du *et al.*, 2011). The 272 nm absorbance peak of the 2,4-dichloroquinone product was monitored *versus* time (Oberg & Paul, 1985). The initial rate (V) for each reaction was calculated from the linear initial portion of the trace automatically using the *Cary Win UV* software set to kinetic mode. All of the activity assays of Mb were measured at the optimum pH of 5.4 in 50 m*M* sodium citrate buffer. To measure the turnover number ($k_{\rm cat}$), TCP was added to Mb before the addition of various concentrations of hydrogen peroxide (the final concentrations were 150 µ*M* for TCP, 5 µ*M* for Mb and 0–6.4 m*M* for H_2O_2). To determine the $K_{\rm m}$ for TCP, varied concentrations of TCP were mixed with Mb and the reactions were then initiated by addition of H_2O_2 (the final concentrations were 0–0.25 m*M* for TCP, 5 µ*M* for Mb and 1.6 m*M* for H_2O_2). The initial rates as a function of H_2O_2 or TCP concentration were fitted to the Michaelis–Menten equation or to the sigmoidal allosteric model using *GraphPad Prism* 5.

2.5. O_2-dissociation constant determination

O_2-dissociation equilibrium constants (K_{O_2}) for Mb and its variants in the ferrous state were determined as recently described in detail by Sun *et al.* (2014). Briefly, the method developed by Makino & Yamazaki (1974) was used; it depends on first measuring a partition constant for the replacement of the bound O_2 in oxyferrous protein by isocyanide ligand and then a dissociation constant for an isocyanide ion bound to deoxyferrous protein.

2.6. Molecular electrostatic potential calculations

Calculations of the molecular electrostatic potential were carried out using *DelPhi* (Rocchia *et al.*, 2001) with dielectric constants of 2.0 and 78 for the protein and solvent, respectively, and an ionic strength of 0.1 *M*.

3. Results and discussion

3.1. Overall structures

K42Y and K42N crystallize in different space groups, $P2_12_12_1$ and $P6$, respectively, with different solvent contents of 40 and 60%, respectively. An interaction between the hydroxyl group of Tyr42 and the N-terminus of a neighboring molecule, which cannot be formed in K42N, is likely to be the main factor leading to the different crystal packing.

Table 2
Comparison of selected distances at the heme for aquo-Mb (1a6k, X-ray structure; 1l2k, neutron structure at room temperature), K42N and K42Y.

	Wild-type Mb (1a6k)	Wild-type Mb (1l2k)	K42N	K42Y
Fe–His89 $N^{\varepsilon 2}$ (Å)	2.14	2.22	2.09	2.10
Fe–His55 $N^{\varepsilon 2}$ (Å)	4.30	4.42	4.36	4.40
Fe–water (Å)	2.13	2.21	2.09	2.10
His55 $N^{\varepsilon 2}$–water (Å)	2.67	2.72	2.83	2.83
Fe–His55 C^{α} (Å)	8.56	8.68	8.63	8.64

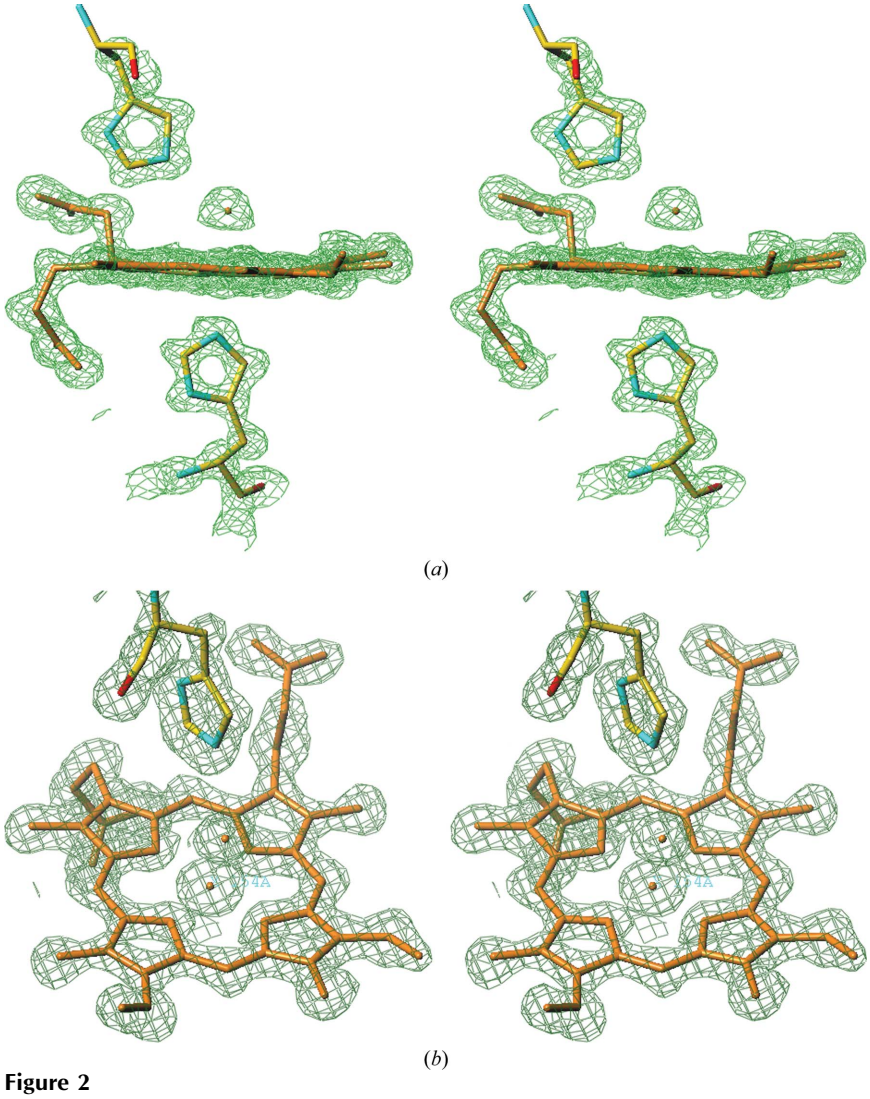

Figure 2
Stereoview of representative electron density from final $2F_o - F_c$ maps. The heme environment is shown in (*a*) K42N contoured at the 1.5σ level and (*b*) K42Y contoured at the 1.3σ level. The relevant distances are listed in Table 2 and are shown in Supplementary Figs. S3 and S4.

The final model of K42N contains all of the residues including the N-terminal methionine, heme, five sulfate ions, three ethylene glycol molecules and 304 water molecules. The quality of the electron-density maps was very good, and the heme environments of K42N and K42Y are shown in Fig. 2. In general, the K42Y and K42N structures are similar to that of aquo-Mb (PDB entry 1a6k; Vojtechovsky *et al.*, 1999), with 0.70 and 0.48 Å r.m.s. deviations in C^{α} positions, respectively; the r.m.s. deviation between K42Y and K42N is 0.71 Å. Their superposition is shown in Supplementary Fig. S1. The larger deviations are likely to result from the different crystal packing affecting the molecular structures.

3.2. Heme environment

The heme environments in K42Y and K42N superposed with that of Mb are shown in Fig. 3. The heme may be reduced and in the metastable aquo ferrous state (Hersleth *et al.*, 2008), but for our comparative analysis of peroxidase function this probably has only a small effect since all of the structures are likely to be affected in a similar way. The individual structures of this region are shown in Supplementary Figs. S2, S3 and S4. The distances at the heme in K42N and K42Y are compared with those in Mb in Table 2. It has been proposed, as reviewed recently by Hersleth *et al.* (2008), that the major factor causing lower rates of peroxidase activity in Mb than in classical peroxidases is the lack of two residues: the Asp that forms the hydrogen bond to the proximal His (Sono *et al.*, 1996) and the distal Arg that stabilizes the negative charge on the leaving group (Poulos & Kraut, 1980). Also, the shorter distance between the distal His and the heme Fe in Mb was considered to affect acid–base catalysis, leading to the heterolytic cleavage of hydrogen peroxide (Matsui *et al.*, 1999). The structures reported here suggest a mechanism for this phenomenon: the closer approach of the distal His results in the stabilization of the water molecule coordinated to Fe. The hydrogen-bonding distance of ∼2.83 Å between N^{ε} of His64 and the water coordinated to Fe in K42Y and K42N is 0.15 Å longer than this distance in Mb (2.67 Å). Thus, the weaker hydrogen bond between the distal histidine and the Fe-coordinated water should facilitate the replacement of this water by hydrogen peroxide and contribute to the increased peroxidase activity. This is consistent with the trend observed for wild-type aquo-DHP, in which the distance from N^{ε} of His64 to the coordinated water is fairly long (3.1 Å), while the peroxidase activity is relatively

Table 3
Turnover numbers (k_{cat}) of Mb variants and DHP for the TCP dehalogenation reaction in 50 m*M* sodium citrate pH 5.4 and their O_2 affinities (K_{O_2}) in 100 m*M* potassium phosphate buffer pH 7.0 at 4°C.

The k_{cat} values for Mb, DHP A and F43H/H64L Mb are from Du *et al.* (2011). The K_{O_2} values for Mb, F43H/H64L Mb and DHP A are from Sun *et al.* (2014).

Protein	K_{O_2} (m*M*)	$k_{cat}^{H_2O_2}$ (min^{-1})	Fe–His55 $N^{\varepsilon 2}$ (Å)	His55 $N^{\varepsilon 2}$–water (Å)
Mb	0.27 ± 0.01	19 ± 2	4.30	2.67
K42Y Mb	0.19 ± 0.006	67 ± 3	4.39	2.82
K42N Mb	0.32 ± 0.01	104 ± 5	4.36	2.84
F43H/H64L Mb	6.12 ± 0.60	161 ± 9	5.4	4.61†
DHP A	3.23 ± 0.37	243 ± 3	5.4	3.10

† The interaction is mediated by another water molecule.

high. A comparison of distances and peroxidase activity is shown in Table 3. Classical peroxidases typically have pentacoordinated ferric heme with no distal water bound at room temperature (Dunford, 1999).

For optimal distal water molecule binding to the heme iron in ferric Mb, an interaction with the distal histidine is essential. Replacement of the histidine with a hydrophobic residue leads to pentacoordinated ferric heme at room temperature (Quillin *et al.*, 1993; Engler *et al.*, 2003). Thus, for the previously identified correlation of peroxidase activity with longer Fe–distal histidine distance (Matsui *et al.*, 1999), the weaker distal water binding appears to be a major factor. This point of view is supported by studies of the double Mb mutant F43H/H64L, in which the distal pocket is very different from that in wild-type Mb, yet the peroxidase activity is approximately eight times higher (Matsui *et al.*, 1999). In this mutant, the distal histidine present in a new position only interacts with the distal water indirectly through another water molecule. Also, upon addition of H_2O_2 to ferric Mb, compound II (Mb II) and a protein radical were observed rather than compound I (Mb I) and it was rationalized that the decay of Mb I is much faster than its formation (Matsui *et al.*, 1999). However, for the more active mutant F43H/H64L and a very high concentration of 0.5 m*M* H_2O_2 formation of Mb I was observed. Likewise, F43H/H64L dismutated H_2O_2 to molecular oxygen and water at a 50-fold higher rate than wild-type Mb (Matsui *et al.*, 1999). Apparently, the peroxidase activity tolerates the active-site restructuring in F43H/H64L very well while profiting from the weaker distal water binding. Thus, it appears likely that the increased peroxidase function observed in the Mb Lys42 variants studied here is also primarily owing to weaker binding of the distal water.

Why the mutation of Lys42 weakens the distal water binding is not obvious. The distances between C^{α} of the distal histidine and Fe in the mutants are 8.63 and 8.64 Å, which are almost the same as in oxy-Mb (8.66 Å) but longer than the 8.56 Å distance that is observed in aquo myoglobin. It appears unlikely that the K42N or K42Y mutations somehow rigidify the molecule and prevent it from forming a strong distal histidine–water interaction. Rather, the changes in the His64 C^{α} position are in response to the side-chain interaction with the heme ligand. This leaves electrostatics as a likely explanation. In the structure of aquo metmyoglobin determined by neutron diffraction (PDB entry 1l2k), the $N^{\varepsilon 2}$ atom of the distal histidine is not protonated and serves as the acceptor of a hydrogen bond from the distal water (Ostermann *et al.*, 2002). The longer hydrogen bonds between His64 $N^{\varepsilon 2}$ and the distal water observed in the mutant structures, 2.83 Å, are in agreement with the typical length of the N—H···O bond of 2.88 Å (Jeffrey & Saenger, 1991). Therefore, a possible explanation is that the mutation affects the protonation equilibrium of the distal histidine (at $N^{\varepsilon 2}$ or $N^{\delta 1}$) and leads to a reversal of the roles in the hydrogen bond, with the water molecule functioning as the donor in Mb (O—H···$N^{\varepsilon 2}$) and the acceptor (O···H—$N^{\varepsilon 2}$) in the mutants (and DHP). The distance between the ammonio group of Lys42 and His64 $N^{\varepsilon 2}$ is 13.7 Å and it is the heme which is between these moieties (Fig. 3). Our calculations of molecular electrostatic potential showed a change of $-0.70kT\,e^{-1}$ for $N^{\varepsilon 2}$ and $-0.36kT\,e^{-1}$ for $N^{\delta 1}$ upon elimination of the lysine charge, which corresponds to shifts in the pK_a of 0.30 and 0.15, respectively (Kreij *et al.*, 2002). A neutron study and/or more accurate calculations that would take into consideration the effects of the heme could prove this hypothesis. The pK_a of the water coordinated to Fe in ferric Mb is 8.3 (Kobayashi *et al.*, 1982) and the mutation makes it even less acidic (the calculated pK_a shift is 0.54), so the water/hydroxide equilibrium cannot be responsible for the observed effect.

3.3. Mutation site

Lys42 is in the extended environment of the heme (see Supplementary Fig. S1). Its NH_3 moiety forms a 2.72 Å hydrogen bond to the carbonyl of Lys98 in Mb (Supplementary Fig. S2). An equivalent interaction is not present upon the replacement of Lys42 by either tyrosine or asparagine. The side chains of Tyr42 and Asn42 do not directly form hydrogen

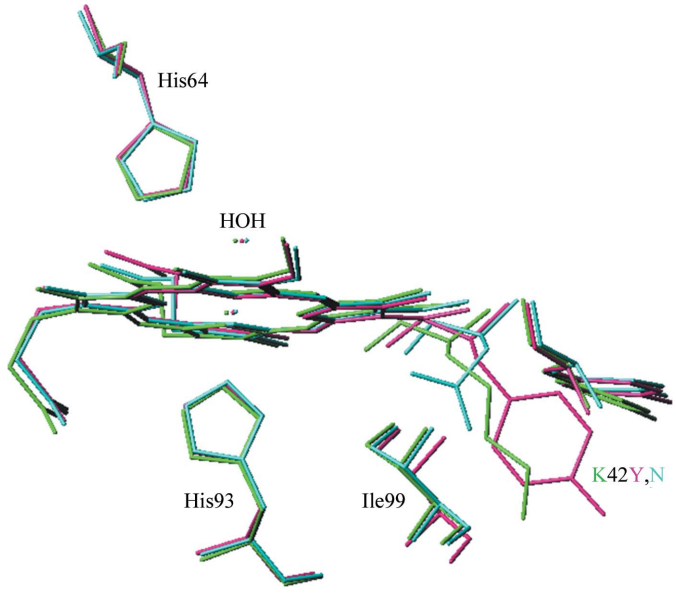

Figure 3
Superposition of wild-type Mb (green; PDB entry 1a6k), K42Y Mb (pink) and K42N Mb (turquoise). The neighboring amino acids affected by the mutations are included.

bonds to the surrounding amino acids. Rather, it appears that water molecules mediate the hydrogen bonding of Tyr42 and Asn42 to other amino acids. In the structure of K42Y the hydroxyl of Tyr42 forms a 2.68 Å hydrogen bond to a water molecule, which forms another 2.77 Å hydrogen bond to the side chain of Tyr103 (Supplementary Fig. S3). In the structure of K42N a new hydrogen bond was generated involving NH_2 of Asn42 and a water molecule, which in turn forms a 2.88 Å hydrogen bond to the carbonyl of His97 (Supplementary Fig. S4). Notably, the hydrophobic residues Ile99 and Tyr103 around the mutation site were also slightly affected, which in turn probably modulates the heme environment. In particular, in K42N the side chain of Asn42 turns to face the pyrrole plane and is closer to the heme.

3.4. Peroxidase activity

Kinetic data for the dehalogenation of TCP are included in Table 3. Comparison of the k_{cat} values shows a ∼3.5-fold higher peroxidase activity for K42Y than for Mb. The activity of K42N is enhanced even more by ∼5.5-fold relative to Mb; this trend parallels the activity of the corresponding DHP enzymes.

3.5. Oxygen-binding affinity

Unlike the peroxidase activity, the oxygen-binding affinity of Mb and K42Y and K32N does not show a trend (see Table 3). This is consistent with dioxygen binding to penta-coordinated ferrous heme and thus no interference by the distal water. The oxygen affinity of the double Mb mutant F43H/H64L is lower by a factor of 23 than that of Mb (Table 3). In contrast, as discussed above, its dehaloperoxidase and catalase activity are eight and 50 times higher than those of Mb, respectively. Thus, the kinetic data and the spectroscopic data showing the formation of compound I by the mutant (Matsui *et al.*, 1999) all indicate that ferric F43H/H64L binds H_2O_2 much better than ferric Mb, while ferrous F43H/H64L binds dioxygen much more poorly than ferrous Mb. For Mb, the binding geometries of O_2 and H_2O_2 are almost identical (Hersleth *et al.*, 2008); it may be expected that for F43H/H64L the geometry of O_2 binding is similar to that of H_2O_2 binding. If so, it is likely that part of the differences in ligand binding to ferric F43H/H64L *versus* ferric Mb can be attributed to the lack of direct interaction of the distal histidine with the water molecule coordinated to the Fe in F43H/H64L and the consequent weaker distal water stabilization.

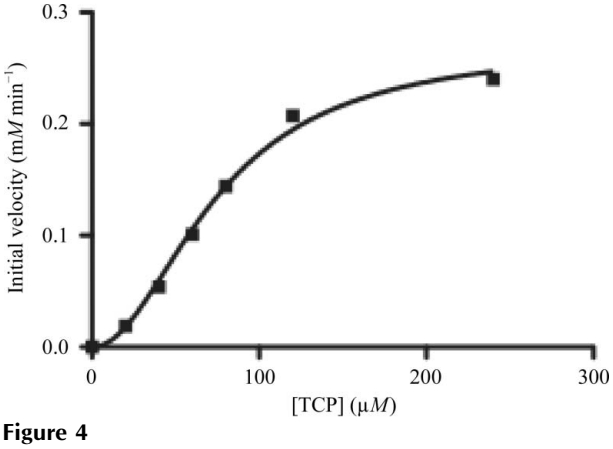

Figure 4
The dehaloperoxidase kinetics of K42N Mb as a function of TCP concentration in 50 mM citrate buffer pH 5.4 at 4°C. The curve represents the best fit to the allosteric sigmoidal model $V = V_{max}[TCP]^2/\{(K_{1/2})^2 + [TCP]^2\}$.

3.6. Cooperativity in K42N

Interestingly, the initial rates for K42N when its activity was measured as a function of TCP concentration fitted better to the allosteric sigmoidal equation than to the standard Michaelis–Menten equation. The sigmoidal curve indicated strong positive cooperativity in K42N Mb. The best fit to the allosteric sigmoidal model $V = V_{max}[TCP]^h/\{(K_{1/2})^h + [TCP]^h\}$, shown in Supplementary Fig. S5, yielded the following values (with the last digit in parentheses giving the standard deviation): V_{max} = 0.259 (9) mM min^{-1}, h = 2.4 (2), $K' = (K_{1/2})^h$ = 26 (20) μM. Previous studies showed that Mb dimerizes by forming a dityrosine cross-link in the presence of H_2O_2 (Detweiler *et al.*, 2005; Tew & Ortiz de Montellano, 1988; Gunther *et al.*, 1998). A computer docking experiment and mass-spectrometric analysis showed a dityrosine covalent bond between Tyr151 of one Mb monomer and Tyr103 of the other (Tew & Ortiz de Montellano, 1988). Since the value of the Hill coefficient, h, for a dimer is limited to 2, we have refitted the sigmoidal model with h = 2. The fit, shown in Fig. 4, produced the parameters V_{max} = 0.271 (9) mM min^{-1} and K' = 5.6 (6) μM.

To check whether K42N monomer aggregation is indeed driven by H_2O_2 rather than by TCP, size-exclusion chromatographic analysis was conducted in the presence and absence of 100 mM TCP (Supplementary Fig. S6). The elution volumes of K42Y and K42N with and without TCP are the same within experimental error, indicating that their molecular weights are almost the same and that no monomer aggregation occurs upon TCP binding. The co-crystallization of K42N with TCP was also attempted and the structure of K42N co-crystallized with TCP did not show any differences when compared with the structure of native K42N. Thus, the phenomenon of positive cooperativity of K42N is not owing to oligomerization induced by the presence of TCP substrate.

The K42Y mutant kinetic data fit to the Michaelis–Menten model, as shown in Supplementary Fig. S7. Tyr103, which participates in dityrosine bond formation, and the 42 mutation site are very close (Supplementary Fig. S8). When compared with lysine in Mb and tyrosine in K42Y, the relative small side chain of asparagine in K42N apparently reduces the steric hindrance and facilitates cross-linking between Tyr103 and Tyr151. The positive cooperativity of K42N Mb in the dehalogenation reaction is thus likely to be linked to its dimerization in the presence of excess H_2O_2. Since this appears to be a rare case of engineered cooperativity, which we admit was quite serendipitous, further studies of this phenomenon may be worth pursuing.

4. Conclusions

We prepared two sperm whale Mb mutants, K42Y and K42N, designed to mimic the presence of Asn34 and Tyr34 at the structurally analogous positions in DHP A and DHP B, respectively. The mutants are better peroxidases than Mb, as predicted. The structures of these two Mb mutants reveal changes relative to wild-type Mb that are likely to be associated with the increased peroxidase activity. The hydrogen-bonding networks in the vicinity of the heme are slightly altered owing to the mutations. The distal histidine in the K42Y and K42N Mb mutants is located further from the heme iron and the hydrogen-bonding distances between the Fe-coordinated water molecule and the distal histidine His55 are longer. The weaker binding of the distal water molecule facilitates H_2O_2 binding and is likely to be the mechanism by which the longer distance between the distal histidine and the heme iron enhances the peroxidase function of globins.

In addition, in K42N we observed positive cooperativity for the dehaloperoxidase reaction as a function of TCP concentration. This effect may be explained by the formation of a covalent dimer *via* a dityrosine linkage facilitated by the replacement of Lys42 with the smaller asparagine.

Financial support was provided by the National Science Foundation (MCB 0820456). Data were collected on the SER-CAT 22-ID beamlines at the Advanced Photon Source, Argonne National Laboratory. Use of the Advanced Photon Source was supported by the US Department of Energy, Office of Basic Energy Sciences under Contract No. W-31-109-Eng-38.

References

Antonini, E. & Brunori, M. (1971). *Hemoglobin and Myoglobin in their Reactions with Ligands.* Amsterdam: North-Holland.
Chen, Y. P., Woodin, S. A., Lincoln, D. E. & Lovell, C. R. (1996). *J. Biol. Chem.* **271**, 4609–4612.
Detweiler, C. D., Lardinois, O. M., Deterding, L. J., de Montellano, P. R., Tomer, K. B. & Mason, R. P. (2005). *Free Radic. Biol. Med.* **38**, 969–976.
Draghi, F., Miele, A. E., Travaglini-Allocatelli, C., Vallone, B., Brunori, M., Gibson, Q. H. & Olson, J. S. (2002). *J. Biol. Chem.* **277**, 7509–7519.
Du, J., Huang, X., Sun, S., Wang, C., Lebioda, L. & Dawson, J. H. (2011). *Biochemistry*, **50**, 8172–8180.
Du, J., Sono, M. & Dawson, J. H. (2010). *Biochemistry*, **49**, 6064–6069.
Dunford, H. B. (1999). *Heme Peroxidases*. New York: Wiley.
Emsley, P., Lohkamp, B., Scott, W. G. & Cowtan, K. (2010). *Acta Cryst.* D**66**, 486–501.
Engler, N., Prusakov, V., Ostermann, A. & Parak, F. G. (2003). *Eur. Biophys. J.* **31**, 595–607.
Franzen, S., Roach, M. P., Chen, Y. P., Dyer, R. B., Woodruff, W. H. & Dawson, J. H. (1998). *J. Am. Chem. Soc.* **120**, 465–4661.
Franzen, S., Thompson, M. K. & Ghiladi, R. A. (2012). *Biochim. Biophys. Acta*, **1824**, 578–588.
Gunther, M. R., Tschirret-Guth, R. A., Witkowska, H. E., Fann, Y. C., Barr, D. P., Ortiz De Montellano, P. R. & Mason, R. P. (1998). *Biochem. J.* **330**, 1293–1299.
Hersleth, H. P., Hsiao, Y. W., Ryde, U., Görbitz, C. H. & Andersson, K. K. (2008). *Chem. Biodivers.* **5**, 2067–2089.
Huang, X., Wang, C., Celeste, L. R., Lovelace, L. L., Sun, S., Dawson, J. H. & Lebioda, L. (2012). *Acta Cryst.* F**68**, 1465–1471.
Jeffrey, G. A. & Saenger, W. (1991). *Hydrogen Bonding in Biological Structures*. Berlin: Springer.
Kabsch, W. (1976). *Acta Cryst.* A**32**, 922–923.
Kobayashi, K., Tamura, M. & Hayashi, K. (1982). *Biochemistry*, **21**, 729–732.
Kreij, A. de, van den Burg, B., Venema, G., Vriend, G., Eijsink, V. G. & Nielsen, J. E. (2002). *J. Biol. Chem.* **277**, 15432–15438.
LaCount, M. W., Zhang, E., Chen, Y. P., Han, K., Whitton, M. M., Lincoln, D. E., Woodin, S. A. & Lebioda, L. (2000). *J. Biol. Chem.* **275**, 18712–18716.
Lebioda, L. (2000). *Cell. Mol. Life Sci.* **57**, 1817–1819.
Lebioda, L., LaCount, M. W., Zhang, E., Chen, Y. P., Han, K., Whitton, M. M., Lincoln, D. E. & Woodin, S. A. (1999). *Nature (London)*, **401**, 445.
Makino, R. & Yamazaki, I. (1974). *Arch. Biochem. Biophys.* **165**, 485–493.
Matsui, T., Ozaki, S., Liong, E., Phillips, G. N. Jr & Watanabe, Y. (1999). *J. Biol. Chem.* **274**, 2838–2844.
Murshudov, G. N., Skubák, P., Lebedev, A. A., Pannu, N. S., Steiner, R. A., Nicholls, R. A., Winn, M. D., Long, F. & Vagin, A. A. (2011). *Acta Cryst.* D**67**, 355–367.
Oberg, L. G. & Paul, K. G. (1985). *Biochim. Biophys. Acta*, **842**, 30–38.
Osborne, R. L., Coggins, M. K., Walla, M. & Dawson, J. H. (2007). *Biochemistry*, **46**, 9823–9829.
Osborne, R. L., Sumithran, S., Coggins, M. K., Chen, Y. P., Lincoln, D. E. & Dawson, J. H. (2006). *J. Inorg. Biochem.* **100**, 1100–1108.
Ostermann, A., Tanaka, I., Engler, N., Niimura, N. & Parak, F. G. (2002). *Biophys. Chem.* **95**, 183–193.
Otwinowski, Z. & Minor, W. (1997). *Methods Enzymol.* **276**, 307–326.
Poulos, T. L. & Kraut, J. (1980). *J. Biol. Chem.* **255**, 8199–8205.
Qin, J., Perera, R., Lovelace, L. L., Dawson, J. H. & Lebioda, L. (2006). *Biochemistry*, **45**, 3170–3177.
Quillin, M. L., Arduini, R. M., Olson, J. S. & Phillips, G. N. Jr (1993). *J. Mol. Biol.* **234**, 140–155.
Roach, M. P., Chen, Y. P., Woodin, S. A., Lincoln, D. E., Lovell, C. R. & Dawson, J. H. (1997). *Biochemistry*, **36**, 2197–2202.
Rocchia, W., Alexov, E. & Honig, B. (2001). *J. Phys. Chem. B*, **105**, 6507–6514.
Roussel, A. & Cambillau, C. (1989). *Silicon Graphics Geometry Partners Directory*, pp. 77–78. Silicon Graphics, Mountain View, California, USA.
Sono, M., Roach, M. P., Coulter, E. D. & Dawson, J. H. (1996). *Chem. Rev.* **96**, 2841–2888.
Springer, B. A., Egeberg, K. D., Sligar, S. G., Rohlfs, R. J., Mathews, A. J. & Olson, J. S. (1989). *J. Biol. Chem.* **264**, 3057–3060.
Springer, B. A. & Sligar, S. G. (1987). *Proc. Natl Acad. Sci. USA*, **84**, 8961–8965.
Sun, S., Sono, M., Wang, C., Du, J., Lebioda, L. & Dawson, J. H. (2014). *Arch. Biochem. Biophys.* **545**, 108–115.
Tew, D. & Ortiz de Montellano, P. R. (1988). *J. Biol. Chem.* **263**, 17880–17886.
Vojtechovsky, J., Chu, K., Berendzen, J., Sweet, R. M. & Schlichting, I. (1999). *Biophys. J.* **77**, 2153–2174.
Wang, C., Lovelace, L. L., Sun, S., Dawson, J. H. & Lebioda, L. (2013). *Biochemistry*, **52**, 6203–6210.
Winn, M. D. *et al.* (2011). *Acta Cryst.* D**67**, 235–242.
Zhang, E., Chen, Y. P., Roach, M. P., Lincoln, D. E., Lovell, C. R., Woodin, S. A., Dawson, J. H. & Lebioda, L. (1996). *Acta Cryst.* D**52**, 1191–1193.